Numerical analysis of the coherent radiation emission by two stacked Josephson flux-flow oscillators

A. Wallraff, E. Goldobin,[a] and A. V. Ustinov[b]
Institute of Thin Film and Ion Technology, Research Center Jülich (KFA), D-52425 Germany

(Received 16 July 1996; accepted for publication 22 August 1996)

The numerical investigation of the radiation emission by a system of two magnetically coupled, long Josephson junctions is reported. Time-dependent synchronized voltage response in the flux-flow regime is analyzed for the case of in-phase and out-of-phase oscillations in the junctions. Simulations show that Josephson junctions operating in the in-phase flux-flow mode may generate rf radiation power by a factor of more than 4 larger than that of a single Josephson junction. The radiation in the out-of-phase flux-flow mode is characterized by nearly completely suppressed amplitudes of odd harmonics and considerably damped even harmonics as compared to that of a single barrier junction. The dependence of the radiation power on the parameter spread between the junctions is investigated. The advantages of using stacked Josephson junctions as oscillators for the sub-mm wave band are discussed. © *1996 American Institute of Physics.*
[S0021-8979(96)00623-8]

I. INTRODUCTION

Long Josephson junctions (LJJs) operated in the flux-flow mode were found to be attractive for applications such as sub-mm wave-band tunable local oscillators.[1,2] The performance of such an oscillator is limited by the rf power available for pumping a nonlinear detector, e.g., an SIS mixer. It is well known that one can achieve higher radiation power using an array of coherently operating devices. It has been shown theoretically[3] and experimentally[4] that, in a stack of magnetically coupled LJJs, chains of fluxons moving in different layers can be mutually phase locked.

In the simplest case of the twofold Josephson tunnel junction stack, both the in-phase and out-of-phase locked modes can be realized.[3] Both these modes have been observed experimentally in $Nb-(Al/AlO_x-Nb)_2$ stacks.[5] It has been predicted that the in-phase flux-flow mode multiplies the power of flux-flow oscillators,[6,7] whereas using the out-of-phase mode can double the main radiation frequency of the oscillator.[8]

In this work we report systematic, numerical studies of the ac response of twofold stacked oscillators. The first three harmonics of ac voltage are investigated for both the in-phase and out-of-phase flux-flow modes and compared with that of a single LJJ. Moreover, we study the dependence of the ac voltages and its harmonic content on the spread of parameters such as damping and critical current density of the junctions.

The radiated power of the LJJ stack operating in the in-phase, single-fluxon mode was investigated theoretically by Grønbech-Jensen and Blackburn.[7] They discussed only the total emitted power, though for oscillator applications it is very important to know its spectral distribution. In addition, the power emitted by the stack was compared in Ref. 7 with the power of the single, coupled LJJ of the same stack, whereas in practice it is more appropriate to compare it with the power of the single, uncoupled LJJ with the same parameters. Below we will see that this difference is crucial. Stacked LJJs can be described by the model used in Ref. 7 with the magnetic coupling parameter $\Delta<0$. The opposite sign of the coupling parameter $\Delta>0$,[7] which results in the ''hyperradiance'' effect, is physically irrelevant for stacked junctions. In this paper we report on enhanced superradiance for in-phase locked LJJ stacks and propose an explanation different from that of Ref. 7.

The paper is organized in the following way: The basic equations describing the physical system are introduced in Sec. II, followed by a presentation of the simulation techniques in Sec. III. In Sec. IV, simulation results for flux-flow modes in single uncoupled Josephson junctions and for double junction stacks are presented. Finally, conclusions are given in Sec. V.

II. THEORETICAL MODEL

The theoretical model describing the dynamics of N-fold stacks of magnetically coupled LJJs was developed by Sakai, Bodin, and Pedersen.[9] In the present work we apply their model to twofold stacks and extend it including the case of LJJs with arbitrary parameters. The system of partial differential equations (PDEs) describing the dynamics of the stack is

$$\begin{aligned}
\frac{1}{1-S^2}\,\lambda_J^{A^2}\phi_{xx}^A &= \sin\,\phi^A+\frac{1}{\omega_p^{A^2}}\,\phi_{tt}^A+\frac{1}{\omega_c^A}\,\phi_t^A-\frac{j^A}{j_c^A}\\
&\quad+\frac{S}{j_c^A(1-S^2)\sqrt{d'^A d'^B}}\,\frac{\Phi_0}{2\pi}\,\phi_{xx}^B;\\
\frac{1}{1-S^2}\,\lambda_J^{B^2}\phi_{xx}^B &= \sin\,\phi^B+\frac{1}{\omega_p^{B^2}}\,\phi_{tt}^B+\frac{1}{\omega_c^B}\,\phi_t^B-\frac{j^B}{j_c^B}\\
&\quad+\frac{S}{j_c^B(1-S^2)\sqrt{d'^A d'^B}}\,\frac{\Phi_0}{2\pi}\,\phi_{xx}^A.
\end{aligned}\tag{1}$$

[a]Permanent address: Institute of Radio Engineering and Electronics, Moscow, 103907, Russia.
[b]Electronic mail: a.ustinov@kfa-juelich.de

Superscripts A and B refer either to the junctions A and B, called JJ^A and JJ^B subsequently, or to the bottom and top superconducting electrode. The subscripts x and t indicate partial derivatives. Each equation in the above system of PDEs resembles the usual sine-Gordon equation but includes an additional coupling term proportional to the second derivative of the phase in the neighboring LJJ. The spatial coordinate x and time t in Eq. (1) are given in conventional physical units. The parameter $\lambda_J^{A|B}$ is the Josephson penetration depth of the junction A or B, $\omega_P^{A|B}$ and $\omega_c^{A|B}$ are the plasma frequency and the characteristic frequency, respectively, $d'^{A|B}$ is the magnetic thickness of the corresponding JJ. These parameters are given by the relations

$$\lambda_J^{A|B}=\sqrt{\frac{\Phi_0}{2\pi}\frac{1}{\mu_0 j_c^{A|B} d'^{A|B}}}; \tag{2}$$

$$\omega_p^{A|B}=\sqrt{\frac{2\pi}{\Phi_0}\frac{j_c^{A|B}}{C^{A|B}}}; \tag{3}$$

$$\omega_c^{A|B}=\frac{2\pi}{\Phi_0}R_N^{A|B}j_c^{A|B}; \tag{4}$$

$$d'^{A|B}=\lambda\left(\coth\frac{d^{A|B}}{\lambda}+\coth\frac{d^m}{\lambda}\right), \tag{5}$$

where the superscript m refers to the middle electrode and $d^{A|B|m}$ corresponds to the electrode thickness. The dimensionless coupling parameter S $(-1<S<0)$ is defined in the following way:

$$S=\frac{s_m}{\sqrt{d'^A d'^B}}=-\sqrt{\frac{\sinh\dfrac{d^A}{\lambda}}{\sinh\dfrac{d^A+d^m}{\lambda}}\frac{\sinh\dfrac{d^B}{\lambda}}{\sinh\dfrac{d^B+d^m}{\lambda}}}, \tag{6}$$

where $s_m=-\lambda/\sinh(d^m/\lambda)$. If the junctions are identical, the condition $d'^A=d'^B$ holds and the above definition of S coincides with that of Ref. 3. For the sake of simplicity we rewrite the primary system of PDEs (1) in dimensionless form normalizing all quantities to the parameters of JJ^A. Assuming that the spatial coordinate x is normalized by the Josephson penetration depth λ_J^A and time t is normalized by the inverse plasma frequency $1/\omega_p^A$, we can rewrite Eq. (1) in the form

$$\begin{aligned}
&\frac{1}{1-S^2}\,\phi^A_{\tilde{x}\tilde{x}}=\sin\,\phi^A+\phi^A_{\tilde{t}\,\tilde{t}}+\alpha^A\phi^A_{\tilde{t}}-\gamma\\
&\qquad+\sqrt{\frac{d'^A}{d'^B}}\frac{S}{1-S^2}\,\phi^B_{\tilde{x}\tilde{x}};\\
&\frac{j_c^A}{j_c^B}\frac{d'^A}{d'^B}\frac{1}{1-S^2}\,\phi^B_{\tilde{x}\tilde{x}}=\sin\,\phi^B+\frac{j_c^A}{j_c^B}\frac{C^B}{C^A}\,\phi^B_{\tilde{t}\,\tilde{t}}\\
&\qquad+\frac{j_c^A}{j_c^B}\frac{R^A}{R^B}\,\alpha^A\phi^B_{\tilde{t}}-\frac{j_c^A}{j_c^B}\,\gamma\\
&\qquad+\frac{j_c^A}{j_c^B}\sqrt{\frac{d'^A}{d'^B}}\frac{S}{1-S^2}\,\phi^A_{\tilde{x}\tilde{x}},
\end{aligned} \tag{7}$$

where we introduced the new variables

$$\tilde{t}=\omega_p^A t;\quad \tilde{x}=x/\lambda_J^A;\quad \gamma=\frac{j}{j_c^A}; \tag{8}$$

$$\alpha^{A|B}=\frac{\omega_p^{A|B}}{\omega_c^{A|B}}=\frac{1}{\sqrt{\beta_c^{A|B}}}=\frac{1}{R_N^{A|B}\sqrt{\dfrac{2\pi}{\Phi_0}j_c^{A|B}C^{A|B}}}. \tag{9}$$

The normalized boundary conditions in the case of annular geometry can be written as

$$\begin{aligned}
&\phi^{A|B}|_{\tilde{x}=0}=\phi^{A|B}|_{\tilde{x}=l}-2\pi N^{A|B};\\
&\phi^{A|B}_{\tilde{x}}|_{\tilde{x}=0}=\phi^{A|B}_{\tilde{x}}|_{\tilde{x}=l},
\end{aligned} \tag{10}$$

where $l=L/\lambda_J$, with L being the junction length (circumference). For the linear geometry the boundary conditions in real units are

$$\begin{aligned}
&\phi^A_x|_{x=0,L}=\frac{2\pi}{\Phi_0}H\Lambda^A;\\
&\phi^B_x|_{x=0,L}=\frac{2\pi}{\Phi_0}H\Lambda^B,
\end{aligned} \tag{11}$$

where

$$\Lambda^{A|B}=\lambda\left(\tanh\frac{d^m}{2\lambda}+\tanh\frac{d^{A|B}}{2\lambda}\right). \tag{12}$$

Introducing the normalized units as above we have

$$\begin{aligned}
&\phi^A_{\tilde{x}}|_{\tilde{x}=0,l}=\tilde{H};\\
&\phi^B_{\tilde{x}}|_{\tilde{x}=0,l}=\frac{\Lambda^B}{\Lambda^A}\tilde{H}=\frac{\Lambda^B}{\Lambda^A}\tilde{H},
\end{aligned} \tag{13}$$

where

$$\tilde{H}=\frac{2\pi}{\Phi_0}\Lambda^A\lambda_J^A H=\frac{2H}{H_{c1}^A} \tag{14}$$

is the normalized magnetic field and

$$H_{c1}^A=\frac{\Phi_0}{\pi\Lambda^A\lambda_J^A}=\sqrt{\frac{2\Phi_0 j_c^A}{\pi\lambda\mu_0}}\frac{\sqrt{\coth\dfrac{d^m}{\lambda}+\coth\dfrac{d^A}{\lambda}}}{\tanh\dfrac{d^m}{2\lambda}+\tanh\dfrac{d^A}{2\lambda}} \tag{15}$$

is the first critical field of the single uncoupled JJ^A. In order to simplify the analysis of flux-flow voltages and to avoid complicated interplay[3] between fluxon locking and cavity resonances, we from now on focus on the annular geometry.

III. NUMERICAL PROCEDURE

In experiment, the radiation power of a flux-flow oscillator is expected to be proportional to the square amplitude of the ac voltage at the edge of the LJJ facing an rf coupling circuit, typically, a superconducting microstrip line[1,2] [see Fig. 1(a)]. For a conventional linear LJJ of the length $l\alpha<1$, the ac voltage at the junction edge is rather complicated due to the superposition of fluxon oscillations with cavity resonances (Fiske steps) in the junction. For very long junctions $(l\alpha>1)$ used in nonresonant practical oscillators,[2] only the flux-flow voltage itself is important. In order to save simula-

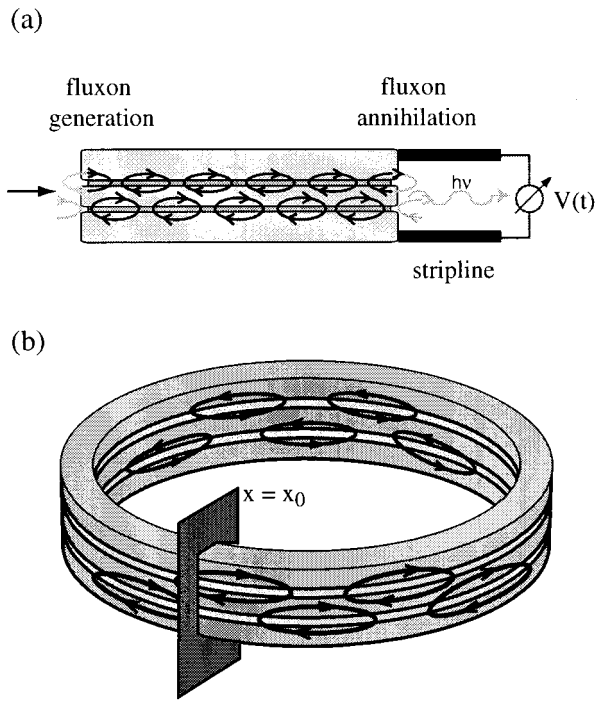

FIG. 1. (a) In a typical experiment, radiation occurs at the edge of a stacked linear oscillator coupled to a microstrip line. (b) In simulations, we calculate the time-dependent voltage in an arbitrarily chosen point $x=x_0$ of an annular stacked junction. The sketch shows a twofold Josephson stack of annular geometry with fluxons moving out of phase.

tion time and simultaneously avoid cavity resonances we carried out most simulations with relatively short junctions ($l=5$) of annular geometry. An example of a twofold stack of this geometry containing out-of-phase, locked fluxons (represented by circulating currents) is shown Fig. 1(b).

For simulations we rewrote Eq. (7) using the notations $R=R^A/R^B$, $J=j_c^A/j_c^B$, $C=C^B/C^A$, and $D'=d'^A/d'^B$ as the measures of the differences in junction parameters which we want to investigate:

$$\begin{aligned}\frac{1}{1-S^2}\,\phi^A_{\tilde{x}\tilde{x}} &= \sin\,\phi^A+\phi^A_{\tilde{t}\,\tilde{t}}+\alpha^A\phi^A_{\tilde{t}}-\gamma \\ &\quad+\sqrt{D'}\,\frac{S}{1-S^2}\,\phi^B_{\tilde{x}\tilde{x}};\\ D'\,\frac{1}{1-S^2}\,\phi^B_{\tilde{x}\tilde{x}} &= \frac{1}{J}\sin\,\phi^B+C\phi^B_{\tilde{t}\,\tilde{t}}+R\alpha^A\phi^B_{\tilde{t}}-\gamma \\ &\quad+\sqrt{D'}\,\frac{S}{1-S^2}\,\phi^A_{\tilde{x}\tilde{x}}.\end{aligned} \tag{16}$$

Equations (16) was solved numerically together with the periodic boundary conditions (10) or (13) using an explicit method treating $\phi_{\tilde{x}\tilde{x}}$ with a five-point, $\phi_{\tilde{t}\,\tilde{t}}$ with a four-point, and $\phi_{\tilde{t}}$ with a three-point symmetric finite difference scheme. Numerical stability was checked by doubling and dividing in half the spatial and temporal discretization steps $\Delta\tilde{x}$ and $\Delta\tilde{t}$ and checking the influence on the fluxon profiles, both in real space and in Fourier space. Stable solutions were achieved for $\Delta\tilde{x}=0.02$ and $\Delta\tilde{t}=0.005$.

Ac voltages were analyzed by simulating the time dependence of the local normalized voltages $V^{A|B}(t)\equiv\phi_t^{A|B}$ at an arbitrarily chosen point $x=x_0$ for annular geometry and at the edge $x=L$ of the stack for linear geometry [see Figs. 1(a) and 1(b)]. To perform spectral analysis of the radiated power, we Fourier transformed the calculated $V(t)$ signal using an FFT algorithm. The FFT transforms were done using 4096 data points acquired at a normalized rate of $1/\delta\tilde{t}=40$, where $\delta\tilde{t}$ is the time step between subsequently sampled points. This choice provided a maximum normalized Nyquist frequency of $\tilde{\nu}_{\max}=20$, which avoided aliasing effects in the spectra. To enhance the amplitude resolution of the obtained spectra, a peak broadening technique[10] with a Gaussian window function was employed. The chosen window function provided a peak amplitude resolution better than 1% and still kept sufficient frequency resolution.

The solutions of the coupled PSGE system were analyzed in the range of $0\leqslant\gamma\leqslant 2$. At $\gamma=0$ the simulations were started with the initial phase distribution of the static case. Then, in each sequential point of the $I-V$ curve, the initial conditions were taken from the stationary state achieved in the previous point. Stationary states were reached by subsequently prolonging the time interval over which the voltage was averaged until the difference from the previous interval was less than 0.01 normalized voltage units. On the resonances this limit was always met after less than 100 normalized time units. All voltages are given in normalized units according to $V=\langle\partial\phi/\partial t\rangle$. Due to the increased computational power needed to calculate the Fourier transforms, we limited ourselves to a discretization step in the bias current of $\Delta\gamma=0.05$. The γ vs V points presented subsequently were interpolated linearly to enhance readability of the plots, which therefore have a ragged appearance in a few cases.

IV. RESULTS

We performed a series of simulations of annular stacks in both in-phase and out-of-phase flux-flow modes. Our main interest was to analyze the influence of the parameter spread (such as damping $\alpha^A\neq\alpha^B$ and critical current density $j_c^A\neq j_c^B$) on the in-phase and out-of-phase locking of junctions. In addition, similar runs were carried out for single uncoupled LJJs which were used for comparison. Results presented in this paper are based on the following set of parameters of the JJs: the length is $L=5\lambda_J^A$ ($l=5$), the number of fluxons trapped in each JJ is $N^A=3$ and $N^B=3$. In annular stacks the number of fluxons is preserved due to the periodic boundary conditions, whereas in linear stacks it is determined by the applied magnetic field H. Unless specified differently, the coupling parameter was always chosen to be $S=-0.4$, which accounts for a moderate coupling. The damping parameter α^A was set to 0.1. The dynamics of the single uncoupled JJ with parameters being equal to those of JJ^A were simulated by setting $S=0$. In this case, the coupling term disappears from Eq. (7) and one obtains two independent, perturbed sine-Gordon equations.

In Fig. 2 the current–voltage characteristics $\gamma(V)$ (IVCs) are shown for a single annular junction and for an annular stack of identical junctions. The asymptotic voltage of the single uncoupled junction (SUJ) shown by the dashed

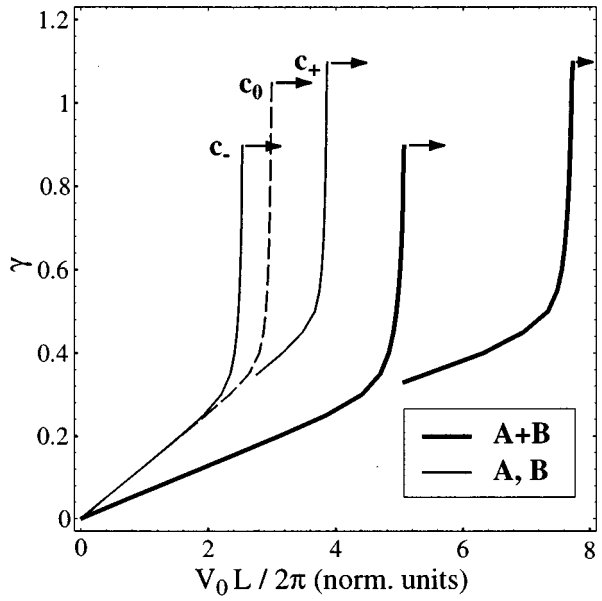

FIG. 2. $I-V$ characteristics of a single uncoupled junction (dashed line) and a stack of two identical coupled junctions (solid lines). Thick solid lines show the total voltage on the stack $V_0^{\Sigma}=V_0^A+V_0^B$.

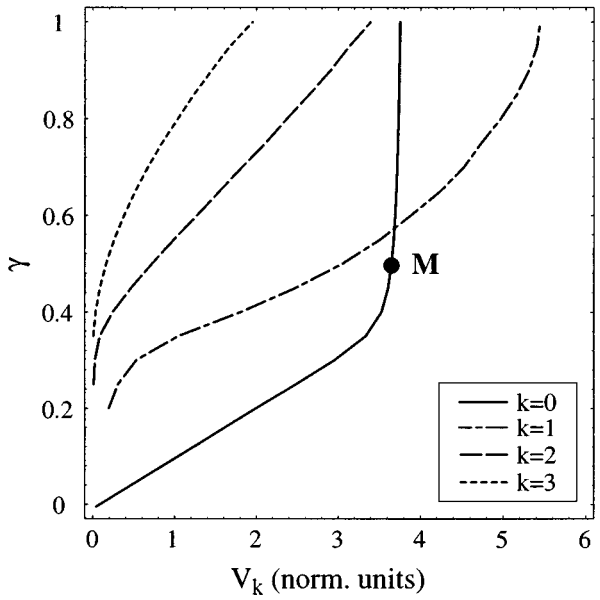

FIG. 3. Dc voltage V_0 (solid line) and amplitudes of the first three harmonics V_1, V_2, and V_3 (dash–dotted lines) vs normalized bias current γ for a single, uncoupled, annular LJJ.

line is determined by $V_0=N\overline{c_0}2\pi/L$, where N is the number of fluxons and $\overline{c_0}$ is the limiting propagation velocity of electromagnetic waves (Swihart velocity) in the junction. In normalized units $\overline{c_0}$ is equal to unity. In the stack with $S\neq 0$, $\overline{c_0}$ splits into two different velocities, $\overline{c_+}$ and $\overline{c_-}$. One can infer the corresponding limiting voltages of the stack from the IVC (solid line) shown in Fig. 2. The lower asymptotic dc voltage of the single coupled junction (SCJ) is given by $V_-=N\overline{c_-}2\pi/L$. The characteristic propagation velocity in the $\overline{c_-}$ (out-of-phase) mode is[3]

$$\overline{c_-}=\frac{\overline{c_0}}{\sqrt{1-S}}<\overline{c_0}. \tag{17}$$

The asymptotic dc voltage $V_+=N\overline{c_+}2\pi/L$ corresponds to the high-velocity $\overline{c_+}$ (in-phase) mode of fluxon motion and is characterized by the limiting velocity:[3,9]

$$\overline{c_+}=\frac{\overline{c_0}}{\sqrt{1+S}}>\overline{c_0}. \tag{18}$$

The dc voltage on the junction is given by the ''0''th harmonic of the voltage $V(t)$. The amplitude of this harmonic V_0 is proportional to the fundamental frequency of the fluxon oscillations through the Josephson relation. In the subsequent sections we analyze the harmonic content of these voltage oscillations.

A. Single uncoupled junction (SUJ)

In this section we present in detail the characteristics of single junctions in order to facilitate coming discussion of stacked junction properties. The simulated dc $I-V$ characteristics $V_0(\gamma)$ of the single-layer, annular, uncoupled LJJ are shown in Fig. 3 by the solid line. The vertical part of this IVC, called flux-flow resonance, is due to relativistic behavior that takes place when the velocity of fluxons u approaches the Swihart velocity $\overline{c_0}$. The asymptotic voltage of the resonance $V=2\pi N\overline{c_0}/L$ corresponds to $u=\overline{c_0}$. For applications, a working point on the $I-V$ curve which guarantees the highest possible radiation power and narrow linewidth[2] has to be chosen at the flux-flow resonance. The spectrum $V(\nu)$ of the ac voltage at the bias point M (see Fig. 3) is shown in Fig. 4. Since we do not include any noise sources in the simulations, the spectrum is discrete and should display zero linewidth for all harmonics. The finite power between the harmonics is a result of the Gaussian

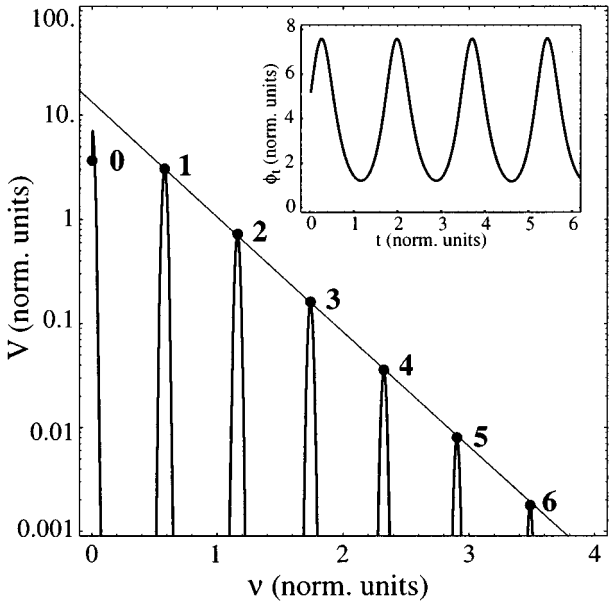

FIG. 4. The voltage spectrum of the single uncoupled annular LJJ at the bias point M (γ=0.5) shown in Fig. 3. The integer numbers are indexing the order k of the harmonics. The solid line follows the exponential decay of harmonic amplitudes for $k\geqslant 1$. In the inset the voltage oscillations $V(t)$ at $x=x_0$ are shown.

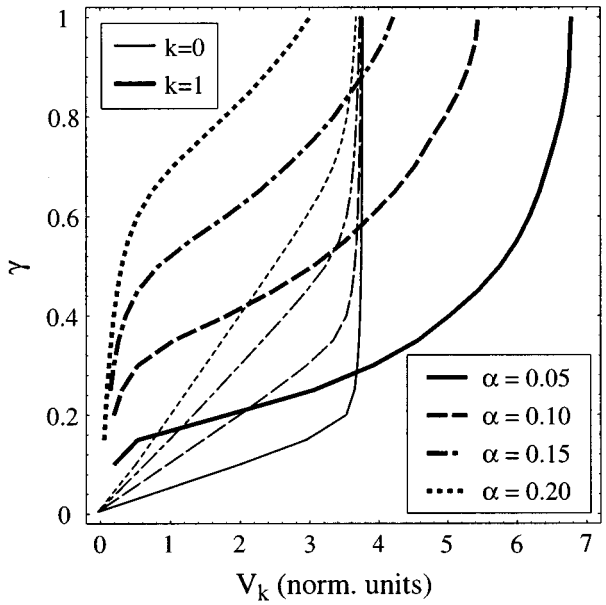

FIG. 5. Dc voltage V_0 and the first harmonic amplitude V_1 vs bias current γ for a single, uncoupled, annular LJJ with damping parameters α=0.05, 0.10, 0.15, and 0.20.

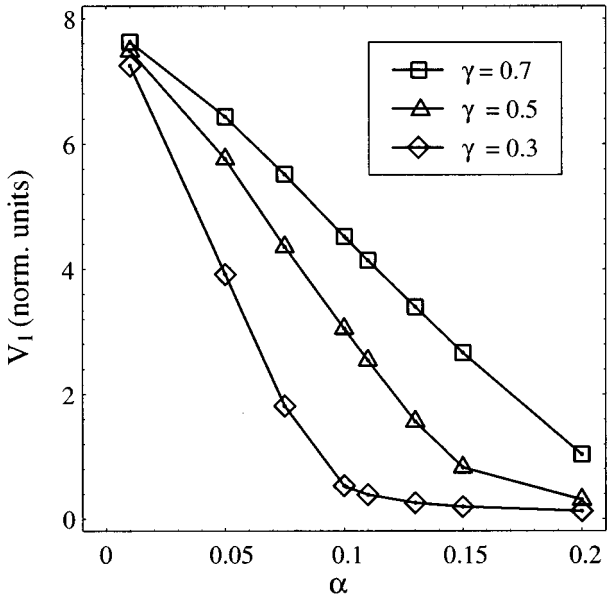

FIG. 6. The amplitude of the first harmonic V_1 at constant levels of γ vs damping parameter α for a single, uncoupled, annular LJJ.

window employed here. The maxima of the Gaussian peaks correspond to the harmonic amplitudes. The time-dependent voltage signal $V(t)$ is shown as an inset. The amplitudes of all harmonics apparently decrease exponentially with their order k, whereas the dc voltage ($k=0$) is fixed by the Josephson relation. The exponential decay of the harmonic amplitudes is an intrinsic feature of the solutions to the unperturbed sine-Gordon equation.

When moving the working point M (Fig. 3) upwards to the top of the resonance, the fluxon voltage pulses are narrowing due to the relativistic Lorentz contraction. Accordingly, the amplitudes of all harmonics in Fig. 4 are increasing. The dependence of the lowest three harmonic voltage amplitudes V_1, V_2, and V_3 (dash–dotted lines) on γ is shown in Fig. 3. Thus, plots in Fig. 3 account for the IVCs of the first four (0th, 1st, 2nd, and 3rd) spectral components of the voltage oscillations in the LJJ. We stress that the spectrum has a high second and third harmonic content near γ=1. This is due to the strongly anharmonic voltage oscillations of the fluxons moving close to the limiting velocity. These harmonic amplitudes are reference values for later comparison to amplitudes of the stacked system.

1. Influence of the damping parameter

Figure 5 shows the dependence of the amplitudes V_0 and V_1 on γ for different values of the damping parameter α. The slope $\Delta I/\Delta U \propto 1/R_N$ of the IVC at low γ is proportional to the damping parameter α as expected. The simulated IVCs for different values of α are in good agreement with the theoretical model by Marcus and Imry:[11]

$$\gamma = \frac{4\alpha}{\pi}\frac{E(k)}{k}\frac{1}{\sqrt{1-u^2}}. \tag{19}$$

The modulus k of $E(k)$ is given by the equation

$$\xi = \frac{L}{N\lambda_J} = 2kK(k)\sqrt{1-u^2}. \tag{20}$$

$K(k)$ and $E(k)$ are the complete elliptic integrals of the first and second kind and ξ is the fluxon spacing in the junction.

The first harmonic amplitude V_1 (Fig. 5) decreases with increasing α, as expected. In Fig. 6 one can see in more detail the dependence of V_1 on α for different fixed values of γ. V_1 decreases linearly with increasing α in a range of γ relatively close to unity. For lower driving currents the dependence is nonlinear. Linear extrapolation of $V_1(\alpha)$ in the range $\alpha<0.075$ results in a limiting first harmonic amplitude at $V_1 \approx 8$ in the limit of $\alpha \to 0$. This feature is rather important, because it allows us to extrapolate the data simulated for $\alpha \approx 0.1$ to values of $\alpha<0.01$ that are more relevant for typical experiments.

2. Influence of the critical current density

To evaluate the influence of spread in critical currents in the coupled system we simulated also the influence of variation of j_c on the ac voltage in SUJs. This was done by choosing $S=0$ and $J \neq 1$ in Eq. (16) and analyzing the voltages in JJ^B. Since $j_c^B = j_c^A/J$, the effective critical current in JJ^B differs from JJ^A by a factor of $1/J$. The dc voltage and the first three harmonics are shown in Fig. 7. For each value of J the characteristics are plotted up to the current at which the junction switches from the flux-flow resonance to higher voltages (McCumber branch). We observe that this switching current scales with $1/J$ as expected from Eqs. (16). Moreover, the fluxons move at higher speeds for lower j_c at the same γ. The dependence of the first harmonic amplitude on $1/J$ at different values of driving current is presented in Fig. 8. We note that the voltage amplitude only weakly depends on $1/J$ at constant values of driving current $\gamma \geqslant 0.3$ in the studied range $0.5<J<2.0$. For large $1/J$ the amplitudes increase with the switching current. In higher harmonics, the junction

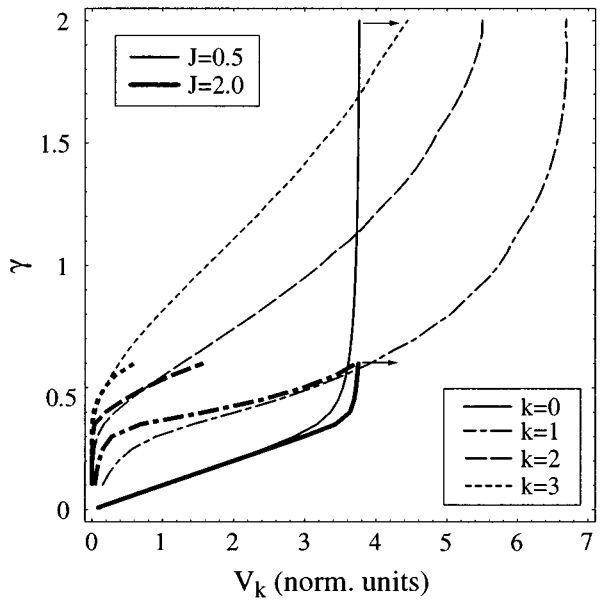

FIG. 7. The dc voltage V_0 and the first three harmonic amplitudes V_1, V_2, and V_3 vs normalized bias current γ for the single, uncoupled, annular JJ^B with $\alpha=0.1$ and critical current parameters $J=j_c^A/j_c^B=0.50$ and 2.00. Arrows indicate switching to higher voltages.

with lower j_c exhibits larger amplitudes at the same driving current. This is because the fluxons in this junction reach the limiting velocity at lower normalized driving current, as can be seen from the dc $I-V$ characteristics in Fig. 7.

B. Out-of-phase mode

The qualitative features of the time-dependent dynamics of symmetric stacks for both the in-phase and out-of-phase modes have been investigated earlier in Ref. 3. Later, the idea of doubling the frequency of Josephson radiation using a stacked flux-flow oscillator operating in the out-of-phase mode was proposed.[8] Here we examine the harmonic content of voltage oscillations in detail.

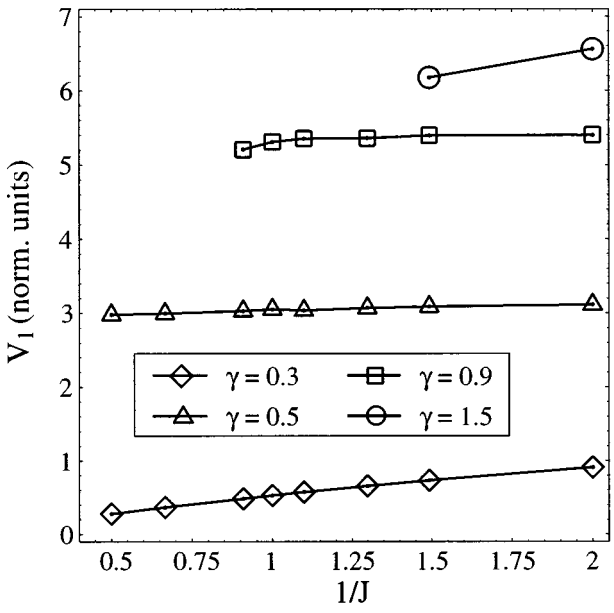

FIG. 8. The amplitudes of the first harmonic V_1 at constant γ vs $1/J=j_c^B/j_c^A$ for the single, uncoupled, annular JJ^B ($\alpha=0.1$).

In the flux-flow resonance, the voltage oscillations $V^A(t)$ in JJ^A and $V^B(t)$ in JJ^B at an arbitrary point $x=x_0$ of the stack are periodic in time. Thus, $V^A(t)$ and $V^B(t)$ can be expanded into Fourier series:

$$V^A(t)=\sum_{k=0}^{\infty} V_k^A \cos(\omega^A k t+\varphi_k^A); \tag{21}$$

$$V^B(t)=\sum_{k=0}^{\infty} V_k^B \cos(\omega^B k t+\varphi_k^B), \tag{22}$$

where $V_k^{A|B}$ are the amplitudes and $\varphi_k^{A|B}$ the phases of the kth harmonics. The fundamental angular Josephson frequencies are given by $\omega^{A|B}$.

If the junctions are frequency locked, their fundamental angular frequencies are identical $\omega^A=\omega^B=\omega$. Accordingly, the sum of the two voltages can be expressed as

$$V^{\Sigma}(t)=\sum_{k=0}^{\infty} |V_k^{\Sigma}|\cos(\omega k t+\vartheta_k), \tag{23}$$

where

$$|V_k^{\Sigma}|^2=V_k^{A^2}+V_k^{B^2}+2V_k^A V_k^B \cos(\Delta\varphi_k) \tag{24}$$

is the square of the total amplitude of the kth harmonic, depending on the respective junction harmonic amplitudes V_k^A and V_k^B and their phase difference $\Delta\varphi_k=\varphi_k^B-\varphi_k^A$. The initial phase ϑ_k fixes the phase relation between the harmonics of the total voltage. ϑ_k is not important to determine the harmonic content of the signal, but necessary to reconstruct the wave form.

1. Equal junction parameters

First, for the sake of simplicity, we assume that the junctions have identical properties so that $V_k^A=V_k^B=V_k$ and $\varphi_k^A=\varphi_k^B=\varphi_k$. In out-of-phase mode the voltage $V^B(t)$ is shifted in time relative to $V^A(t)$ by one-half of the fundamental period $T=2\pi/\omega$:

$$V^A(t)=\sum_{k=0}^{\infty} V_k \cos(\omega k t+\varphi_k), \tag{25}$$

$$V^B(t)=\sum_{k=0}^{\infty} V_k \cos[\omega k(t+T/2)+\varphi_k]$$

$$=\sum_{k=0}^{\infty} V_k \cos(\omega k t+\varphi_k+\pi k). \tag{26}$$

With $\Delta\varphi=\pi k$ and Eq. (24) the total amplitudes V_k^{Σ} can be calculated as

$$|V_k^{\Sigma}|^2=V_k^2+V_k^2+2V_k^2\cos(k\pi)=\begin{cases}0, & k=1,3,5,\ldots,\\ 4V_k^2, & k=2,4,6,\ldots.\end{cases} \tag{27}$$

As a result all odd harmonics cancel and the amplitudes of all even harmonics become twice as large as the amplitudes in a single, coupled junction (SCJ) of the stack. The resulting voltage can be expressed as

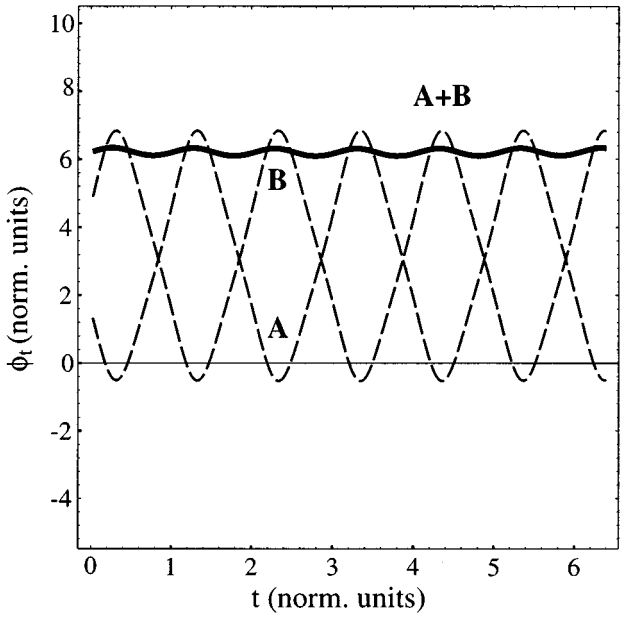

FIG. 9. The time-dependent voltages $V^A(x_0,t)$, $V^B(x_0,t)$, and $V^\Sigma(x_0,t)$ at the arbitarily chosen coordinate x_0 in a stack with equal junction parameters at $\gamma=0.5$.

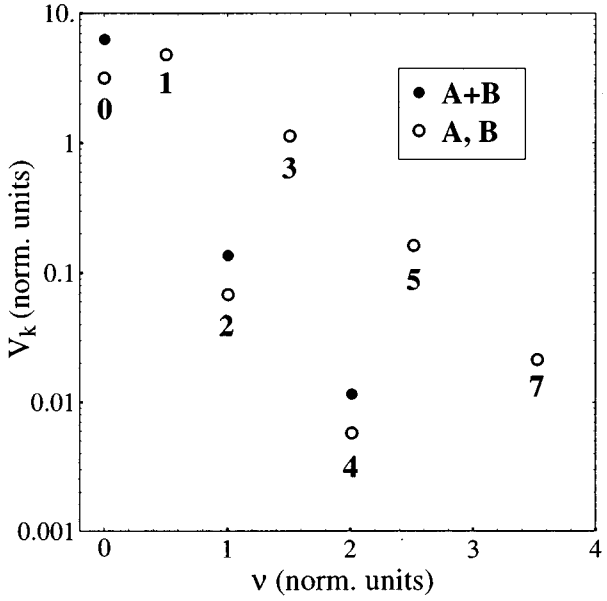

FIG. 10. Spectrum of the voltage oscillations with harmonic amplitudes shown by open circles ($V_k^{A,B}$) and small solid circles (total voltage V_k^Σ) at $\gamma=0.7$. Numbers indicate the harmonic index k.

$$V^\Sigma(t)=\sum_{k=0}^{\infty} 2V_{2k}\cos(2\omega kt+\vartheta_k). \tag{28}$$

Thus one would expect enhanced yield at the second harmonic. In a subsequent section we will analyze the effect of differences in junction parameters on $V^\Sigma(t)$.

In Fig. 9 the voltages $V^A(t)$, $V^B(t)$, and $V^\Sigma(t)$ of a stack with equal junction parameters at $\gamma=0.5$ are plotted versus time. One recognizes that $V^\Sigma(t)$ is governed by a small amplitude oscillation at twice the fundamental Josephson frequency of the stack. The corresponding spectrum of the stack biased at $\gamma=0.7$ is shown in Fig. 10. We note that all odd harmonics of the total voltage V^Σ attain zero amplitudes, in agreement with Eq. (27). The amplitudes of all even harmonics are doubled with respect to the SCJ, but they are much smaller than those of the SUJ. The second harmonic amplitudes of an SUJ (dashed line), an SCJ (solid line), and the stack (thick solid line) in dependence on the bias current γ are shown in Fig. 11. The second harmonic of the SCJ is very much smaller than the second harmonic of the SUJ. This result deserves a more detailed discussion.

Let us compare the spectra shown in Figs. 4 and 10 in more detail. It can be easily noted that the odd harmonic amplitudes of the SUJ are smaller than those of the SCJ. In contrast, the even harmonics in the spectrum of the SCJ are considerably suppressed in comparison to the SUJ. This feature is related to the magnetic coupling between the junctions. Qualitatively, the mechanism responsible for this phenomenon is the following. Due to the coupling, the fluxons moving in JJ^A, with magnetic field profile $\phi_x^A(x)$, create the image profile $\widetilde{\phi_x^A}(x)$ in JJ^B. An example of such an image for $N^A=3$ and $N^B=0$ is shown in Fig. 12. We note that the field profiles are almost identical except for the constant component and the inverted polarity of the profile B. Fourier analysis of the profiles in the master and the image junction has shown that the harmonic content (for $k\geqslant 1$) of the two profiles is almost equivalent for $S=-0.4$ and $\gamma\geqslant 0.3$. Thus, for coupling constants $|S|\geqslant 0.4$, in case of $N^B=0$, we can approximately express the image profile in junction B induced by junction A as

$$\widetilde{\phi_x^A}(x)\approx \text{const}-\epsilon\overline{\phi_x^A}(x), \tag{29}$$

where ϵ is a constant close to but always less than unity. Now, supposing the existence of fluxons also in JJ^B, we obtain in zeroth order approximation

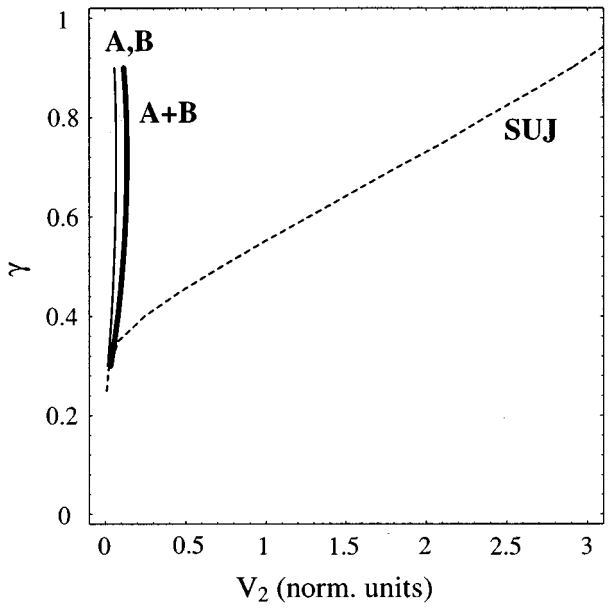

FIG. 11. The amplitudes of the second harmonic V_2 vs bias current γ of the stack of identical junctions synchronized in out-of-phase mode. The dashed line shows V_2 from Fig. 3 of the single uncoupled junction (SUJ) for comparison.

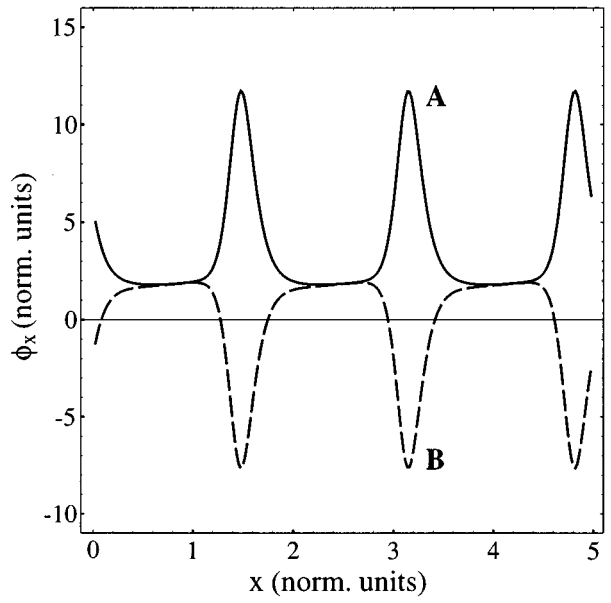

FIG. 12. Magnetic field profiles of the two junctions in the out-of-phase mode biased at $\gamma=0.7$. There are three fluxons trapped in JJ^A; JJ^B contains no net flux.

$$\phi_x^B(x)\approx\overline{\phi_x^B}(x)+\widetilde{\phi}_x^A(x)\approx\overline{\phi_x^B}(x)-\epsilon\overline{\phi_x^A}(x)+\text{const} \quad (30)$$

and a similar expression for $\phi_x^A(x)$. Taking into account the phase difference in the out-of-phase mode $\phi_x^B(x)=\phi_x^A(x-T/2)$ and using the Fourier series expansion of ϕ_x^A one can easily compute the harmonic amplitudes and get expressions similar to Eqs. (25)–(28). First, all odd harmonics of $\phi_x^B(x)$ increase by a factor of $1+\epsilon$. In contrast, all even harmonics of $\phi_x^B(x)$ obtain very small amplitudes of the order of $1-\epsilon$ in comparison to the SUJ. Due to the fact that $\phi^{A|B}(x,t)$ describes traveling waves with the argument $(kx-ut)$, one obtains $V^{A|B}(t)\propto H^{A|B}(x)$, thus the above treatment is applicable to the time-dependent voltages as well. The above considerations well explain the features of the time-dependent voltage signal $V^{\Sigma}(t)$ in Fig. 9 and the voltage spectrum $V(\nu)$ presented in Fig. 10.

Quantitatively, one would have to solve the self-consistent problem for the magnetic field distribution. The analytical expression for the image profiles, derived in Ref. 12 using the perturbation technique, is proportional to S for $|S|\ll 0.1$. Consequently, all spectral components of the image profiles are proportional to S in that range. We have found from numerical simulations of the image profiles that for $|S|\geqslant 0.2$ all harmonic amplitudes are constrained by $0.9V_k^A<V_k^B<V_k^A$ at $\gamma\geqslant 0.3$. This implies that the factor ϵ introduced above is always larger than 0.9. Therefore, the above considerations are appropriate for all experimentally relevant coupling parameters.

We conclude for equal junction parameters that all harmonics (except the dc amplitude V_0) of an SCJ in the out-of-phase flux-flow mode are much smaller in amplitude than the corresponding harmonics of an SUJ. For odd harmonics this phenomenon can be explained by the out-of-phase voltage summation and for even harmonics by the out-of-phase magnetic coupling.

2. Spread in junction parameters

Simulations of stacks with different junction parameters were analyzed in detail. We note that in case of large differences in parameters the mutual phase locking can be difficult or even impossible to achieve. In simulations one can ''artificially'' lock the junctions in some parameter range by choosing appropriate initial conditions. In experiment, phase locking can be facilitated by using an independent magnetic field control for each junction, as demonstrated in Ref. 8.

In the simulations of the out-of-phase flux-flow mode for different junction parameters, the odd harmonics of the total voltage $V^{\Sigma}(t)$ attain nonzero amplitudes. The even harmonic amplitudes become smaller than in the case of equal parameters. This can be explained by considering the general Eq. (24) and allowing different harmonic amplitudes $V_k^{A|B}$ and the phases $\varphi_k^{A|B}$. The resulting amplitudes in the out of phase mode are then given by

$$|V_k^{\Sigma}|^2=V_k^{A^2}+V_k^{B^2}+2V_k^AV_k^B\cos(k\pi+\delta\varphi)$$
$$=\begin{cases}V_k^{A^2}+V_k^{B^2}-2V_k^AV_k^B\cos(\delta\varphi_k), & k=1,3,5,\ldots,\\ V_k^{A^2}+V_k^{B^2}+2V_k^AV_k^B\cos(\delta\varphi_k), & k=2,4,6,\ldots,\end{cases} \quad (31)$$

where

$$\delta\varphi_k=\Delta\varphi_k-k\pi. \quad (32)$$

Thus, the total voltage is determined by the different amplitudes of $V^{A|B}(t)$ and the phase shifts between them. For identical junctions $\delta\varphi_k$ vanishes.

a. Spread in damping. Simulations of the out-of-phase mode were performed for various $R\neq 1$, i.e., different damping coefficients of the two junctions [see Eq. (16)]. The current range at which the phase locking of the junctions takes place is strongly dependent on the ratio of damping parameters of the junctions. A more detailed analysis of this dependence will be presented elsewhere.[13] The data presented here refer to the phase-locked range on the flux-flow resonances.

In general, a spread in damping coefficients leads to an additional decrease of the second harmonic amplitude of the stack. There are two contributions to be considered. First, the fluxon velocity in the coupled system decreases at a given γ when the damping parameter in JJ^B is increased. This contribution is found to be rather small. Second, additional phase shifts $\Delta\varphi_k$ occur between harmonics of the SCJs. As an example we discuss the case $R=1.5$. Figure 13 displays V_2^A, V_2^B, and V_2^{Σ} in dependence on γ, the sum of the first harmonics V_1^{Σ} is shown for comparison. The harmonic amplitudes of each single junction in the stack are identical (see Fig. 13). In general, we found that the SCJ harmonics are almost identical in two junctions for any R examined. Hence, the very small value of V_2^{Σ} has to be the result of an additional phase shift $\delta\varphi_2$ between V_2^A and V_2^B as given by Eq. (32). In the example given in the inset of Fig. 13, the phase shift assumes a value $\delta\varphi_2\geqslant\pi/2$, such that $V_2^{\Sigma}\ll V_2^{A,B}$. The phase in the first harmonic $\delta\varphi_1$ is shifted as well. As a result, the first harmonic amplitude is even larger than the second in this case (see Fig. 13).

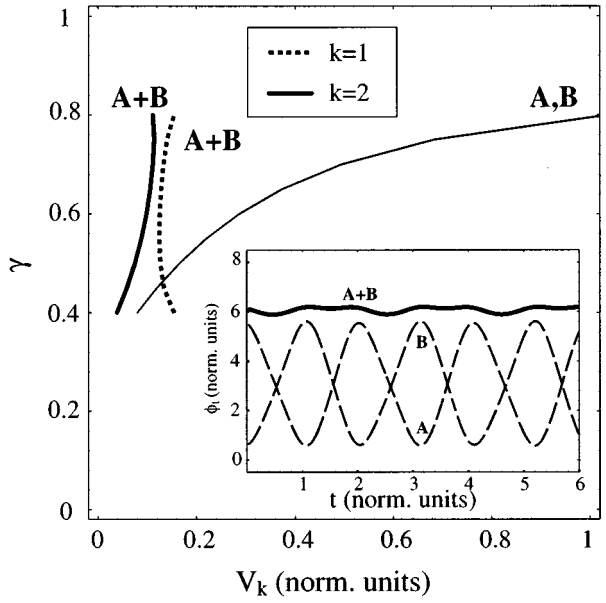

FIG. 13. Solid lines show V_2^A, V_2^B (thin line) and V_2^Σ (thick line) as a function of γ. V_1^Σ (dotted line) is plotted for reference. The voltage profiles $V^A(x_0,t)$, $V^B(x_0,t)$ and $V^\Sigma(x_0,t)$ at $\gamma=0.5$ are shown in the inset.

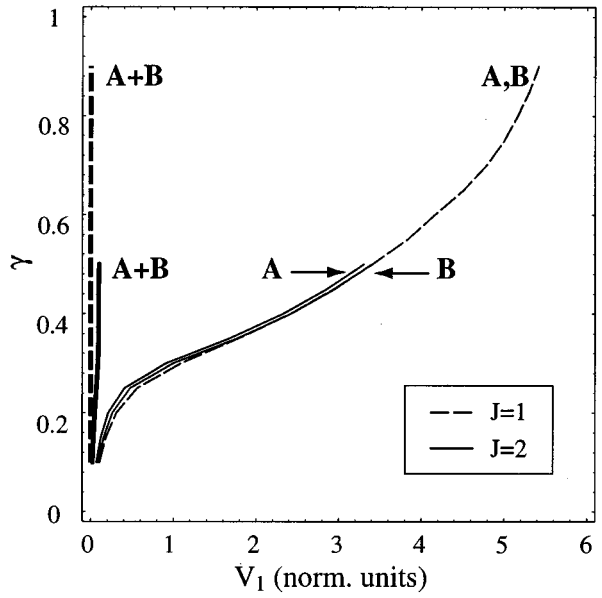

FIG. 15. The first harmonic amplitudes $V_1^{A,B}$ and V_1^Σ plotted vs γ for $J=2$ (solid lines) and $J=1$ (dashed lines).

b. Spread in critical current density. The effect of different critical currents of the two junctions on the out-of-phase mode was investigated for $0.5<J=j_c^A/j_c^B<2.0$ with the fixed coupling strength $S=-0.4$. The calculations for $J\neq 1$ have shown features similar to the behavior for $R\neq 1$ discussed above. In Fig. 14 the time-dependent voltage profiles $V^{A,B}(t)$ and $V^\Sigma(t)$ are plotted for $j_c^A=2j_c^B$. Apparently, the amplitude of the oscillations in each junction are almost identical at this bias current. The Fourier components at the fundamental frequency V_1^A, V_1^B, and V_1^Σ are shown in Fig. 15. The data are plotted for $J=j_c^A/j_c^B=1$ and $J=j_c^A/j_c^B=2$ in dependence on γ. The harmonic amplitudes of the fluxon oscillations in each single junction for $J=1$ are equal, as expected. We found from simulations that for $J=2$ and for all other values of J investigated the ratio of the harmonic amplitudes at resonant voltages is almost equal to unity

$$\frac{V_1^A}{V_1^B}\approx 1. \tag{33}$$

At low bgias currents this ratio agrees with the value expected from the perturbation theory.

In order to discuss Fig. 15 in more detail, we refer to Eq. (31) for $k=1$. Accordingly, the first harmonic amplitude V_1^Σ is given by

$$|V_1^\Sigma|^2=V_1^{A^2}+V_1^{B^2}-2V_1^AV_1^B\cos(\delta\varphi_1). \tag{34}$$

Exact out-of-phase addition of the first harmonic of the two junctions $V_1^\Sigma=V_1^A-V_1^B$ takes place for $\delta\varphi_1=0$. Thus, for junctions with equal critical currents, $V_1^A=V_1^B$ and the sum of the voltages is $V_1^\Sigma=0$ (see Fig. 15). In the case $J\neq 1$, the harmonics V_1^A and V_1^B differ from one another by less than 5%. Additionally, $\delta\varphi_1$ may attain nonzero values. We found that $\delta\varphi_1\leqslant 5°$ for $0.5<J<2.0$ by solving Eq. (34) for $\delta\varphi_1$ and using the simulated values of V_1^A, V_1^B, and V_1^Σ. Thus, $V_1^\Sigma\approx|V_1^A-V_1^B|$ can be applied to all simulated values of J.

Similarly, the second harmonic amplitude V_2^Σ is given by

$$|V_2^\Sigma|^2=V_2^{A^2}+V_2^{B^2}+2V_2^AV_2^B\cos(\delta\varphi_2). \tag{35}$$

Numerical simulations reveal that only for $J=1$ the second harmonic voltages of the two junctions add up in phase ($\delta\varphi_2=0$) in the full current range. As observed also for $R\neq 1$, $\delta\varphi_2$ may attain nonzero values for a spread in critical currents. For $J=1.10$ we observed a transition from $\delta\varphi_2\approx 0$ at $\gamma\approx 0.3$ to $\delta\varphi_2\approx\pi$ at $\gamma\approx 0.8$ while increasing bias current. For larger spread ($J\geqslant 1.30$) the second harmonic amplitudes are

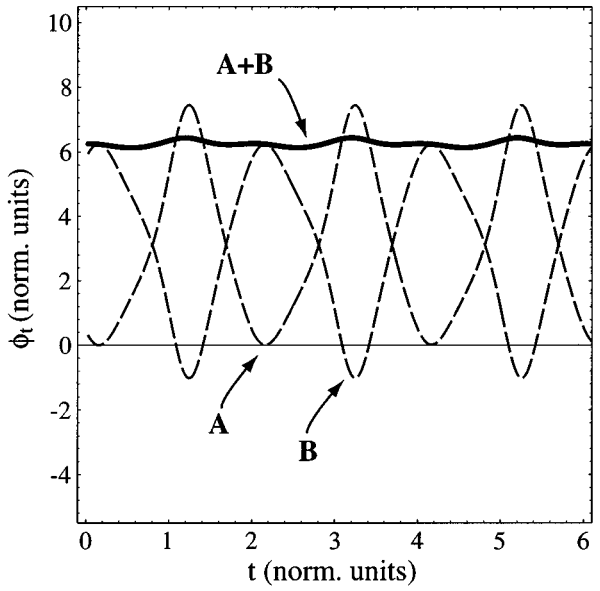

FIG. 14. The evolution of $V^{A,B}(x_0,t)$ and $V^\Sigma(x_0,t)$ in time for $J=j_c^A/j_c^B=2$ at $\gamma=0.5$.

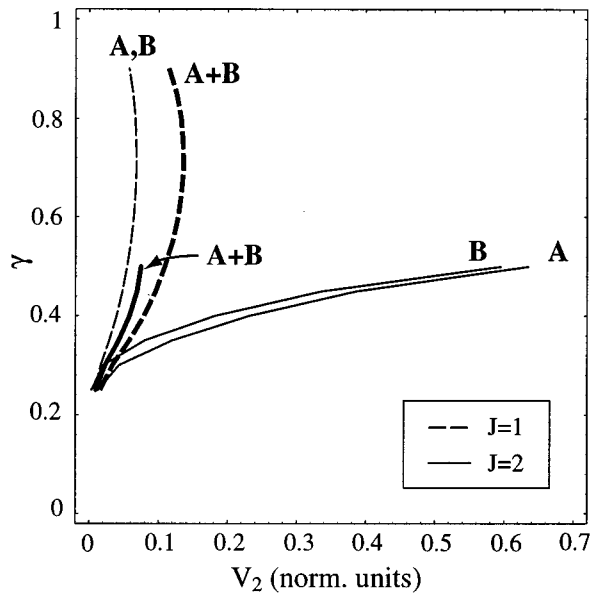

FIG. 16. The second harmonic amplitudes $V_2^{A,B}$ and V_2^{Σ} plotted vs γ for $J=1$ (dashed lines) and $J=2$ (solid lines).

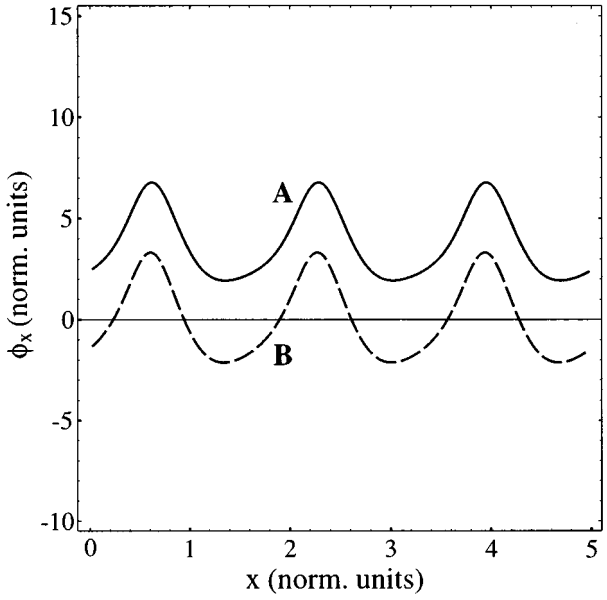

FIG. 17. Normalized magnetic field profiles of junctions A and B at $\gamma=0.7$ in the in-phase mode for $N^A=3$ and $N^B=0$ with coupling constant $S=-0.4$.

out of phase ($\delta\varphi_2\approx\pi$) in the full range of the locked state stability, i.e., $V_2^{\Sigma}\approx|V_2^A-V_2^B|$. An example is given in Fig. 16 for $J=2$ (solid lines). The second harmonic amplitude is suppressed substantially by the occurring shifts $\delta\varphi_2$ which are induced by the spread in critical currents J.

The presented results suggest that stacked flux-flow oscillators operating in out-of-phase mode do not possess any advantages over single, uncoupled LJJ oscillators. We note, however, that our model neglects the surface losses (β term) and the nonlinearity of quasiparticle conductivity α at high frequencies. A correction to the model with $\alpha=$const could be including a damping term $\alpha^{A|B}(x,t)$ depending on the amplitude of the local time-dependent voltage $V^{A|B}(x,t)$. However, such an extension of the model is not very likely to lead to an increase of harmonic amplitudes since the damping increases with frequency. We found this effect in preliminary simulations with nonlinear quasiparticle losses.

C. In-phase mode

For equal JJ parameters, the phases of two junctions biased in the in-phase mode are identical $\phi^A(x)=\phi^B(x)$.[3,9] An analysis using magnetic images equivalent to that of the out-of-phase mode can be applied here as well. In Fig. 17 the magnetic image in JJ^B induced by fluxons in JJ^A is shown. In zeroth order approximation, its amplitude obeys the relation $\tilde{\phi}_x^A\approx\epsilon\phi_x^A-$const, where $0<\epsilon<1$. Accordingly, the profile $\phi_x^B(x)$ in JJ^B is given by

$$\phi_x^B(x)\approx\overline{\phi_x^B}(x)+\tilde{\phi}_x^A(x)\approx\overline{\phi_x^B}(x)+\epsilon\overline{\phi_x^A}(x)-\text{const}. \quad (36)$$

We point out that the summation of the fluxon and the image profile is less accurate than in the out-of-phase case due to the high amplitudes of both $\overline{\phi_x^B}(x)$ and $\tilde{\phi}_x^A(x)$. The identical voltages of individual junctions add up in the in-phase state, which results in an increase of the amplitudes of all harmonics. As an example, the voltage profiles $V^A(t)$ and $V^B(t)$ of equal amplitudes shown in Fig. 18 add up in phase to the voltage profile $V^{\Sigma}(t)$ of a larger amplitude.

Expanding the voltage oscillations in each single junction into a Fourier series and summing the voltages for the in-phase mode, the amplitudes of the resulting signal can be expressed as [see Eqs. (21)–(24)]

$$|V_k^{\Sigma}|^2=V_k^{A^2}+V_k^{B^2}+2V_k^AV_k^B\cos(\delta\varphi_k), \quad (37)$$

$$\delta\varphi_k=\varphi_k^A-\varphi_k^B. \quad (38)$$

Here $\delta\varphi_k$ is the deviation from exact phase matching of each harmonic.

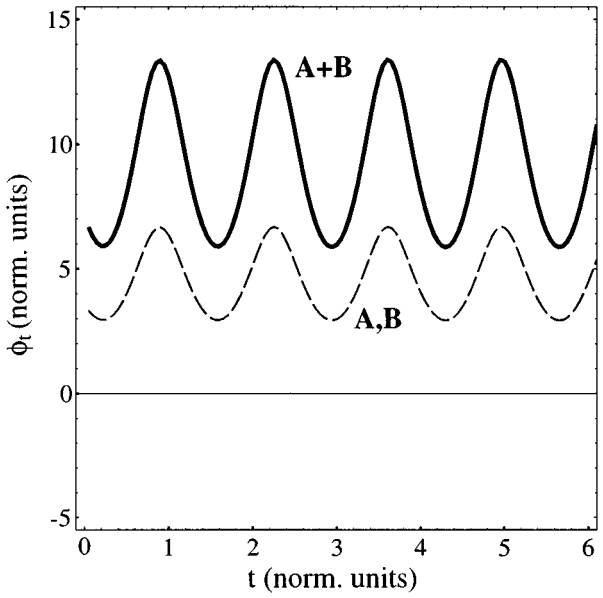

FIG. 18. The time dependent voltages $V^A(x_0,t)$, $V^B(x_0,t)$ and $V^{\Sigma}(x_0,t)$ at $\gamma=0.5$ in in-phase mode.

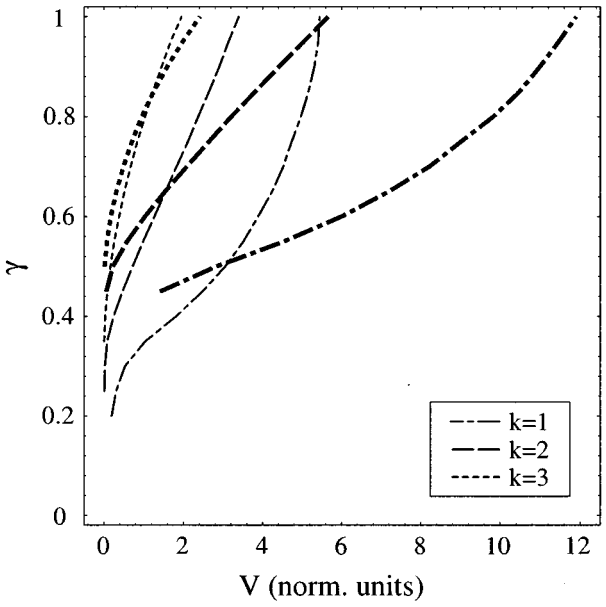

FIG. 19. V_1, V_2, and V_3 of a stack of identical junctions (thick lines) and of the SUJ (thin lines) vs bias current γ in the in-phase flux-flow mode.

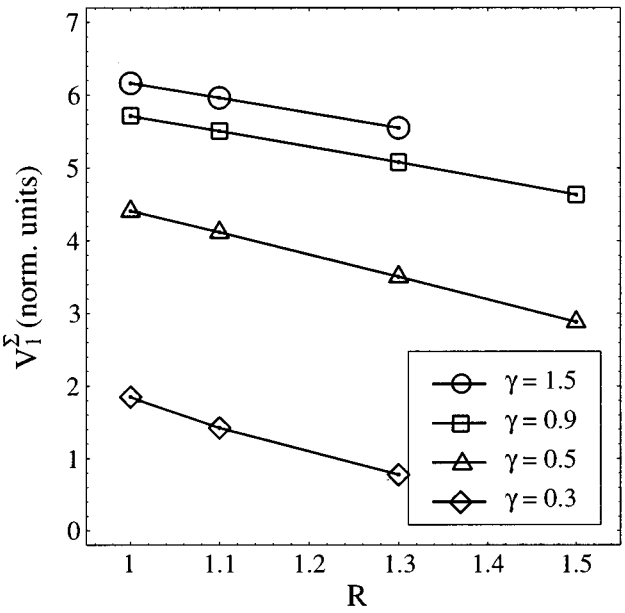

FIG. 20. V_1^Σ at fixed bias values γ vs the ratio of quasiparticle resistances $R=R^A/R^B$ for the in-phase flux-flow mode.

1. Equal junction parameters

The simulated dependence of V_1^Σ, V_2^Σ, and V_3^Σ on γ for the stack of two identical junctions is shown in Fig. 19. For comparison, the SUJ amplitudes V_1, V_2, and V_3 are plotted as well. $V_1^\Sigma(\gamma)$ is nearly equal to the first harmonic amplitude $V_1(\gamma)$ of the SUJ at $\gamma\approx 0.45$ and becomes approximately 2.2 times larger than $V_1(\gamma)$ at $\gamma=1$. The amplitude of the second harmonic V_2^Σ of the stack is equal to V_2 of SUJ at $\gamma\approx 0.6$ and becomes $V_2^\Sigma\approx 1.6V_2$ at $\gamma=1$. Finally, the amplitudes of the third harmonic are approximately equal in the SUJ and the stack. We like to emphasize that, at the top of the resonance, the first harmonic amplitude V_1^Σ is about a factor of 2 larger than V_1, i.e., the radiation power is larger by a factor greater than 4. We suppose that this oversuperradiant effect is due to the redistribution of power between high and low harmonics for SCJs as compared with SUJs.

In addition to the gain in amplitudes, in the in-phase mode we have an increase in frequency $\omega_1^+ = \omega_1^0/\sqrt{1+S} > \omega_1^0$ of all harmonics due to the higher propagation velocity in the c_+ mode. The increase in frequency is determined via the Josephson relation by the dc voltage of the SCJ (see Fig. 2). For $S=-0.4$, the voltage is a factor of $1/\sqrt{1+S} \approx 1.3$ larger due to the enhanced Swihart velocity $\overline{c_+}>\overline{c_0}$.

2. Spread in junction parameters

a. Spread in damping. The dependence of the first harmonic amplitude on the spread in quasiparticle resistances $R=R^A/R^B$ of the two coupled junctions is plotted in Fig. 20. In the studied parameter range, the amplitude V_1^Σ at constant current γ decreases linearly with increasing R. As the amplitudes in JJ^B decrease with respect to JJ^A due to larger damping, the total amplitude V_1^Σ of the coupled system decreases as well. In contrast, for $R^A<R^B$ the amplitude V_1^Σ increases.

In the case of large spread ($R\geqslant 1.2$), the in-phase locked state was found to be impossible to achieve by cycling (with increasing and decreasing γ) through the hysteretic IVC. It can be argued that the junctions do not lock in phase anymore because the fluxon velocities in the two junctions considerably differ from each other at constant γ. Nevertheless, in simulations phase-locking can still be achieved by using the appropriate initial conditions. Thus, the limited stability range is a disadvantage of the in-phase mode as compared with the out-of-phase mode. By increasing the coupling parameter S one can achieve more stable locking even for a larger spread.

b. Spread in critical current density. Simulations of the *in*-phase mode with $J\neq 1$ revealed a similar behavior of voltage amplitudes [Eq. (33)] as discussed above for the out-of-phase mode. The voltage profiles $V^A(t)$, $V^B(t)$, and $V^\Sigma(t)$ for $J=2$ are illustrated in Fig. 21. The amplitudes V_1^A, V_1^B, and V_1^Σ are plotted in Fig. 22 for $J=2$, data for $J=1$ are also shown as a reference. We note that the upper delocking current of the stack is reduced due to the twice-lower critical current of JJ^B. In general, the upper delocking current $j_{\max}$ in the in-phase mode always assumes a value between the single junction critical currents j_c^A and j_c^B. Thus, for $J>1$ the $j_{\max}$ is decreased, whereas for $J<1$ the $j_{\max}$ is increased. As can be seen in Fig. 22, the dependence of V_1^Σ on the bias current γ is almost identical for the two values of $J=1$ and $J=2$. Hence the only substantial change in harmonic amplitude arises from the modified locking range of the stack. This behavior was observed for all values of J where $0.5\leqslant J\leqslant 2$. Figure 23 illustrates the dependence of V_1^Σ on the spread in critical currents J at constant γ. The qualitative behavior is very similar to that of single junctions. For $J<1$ we naturally observed an additional increase in V_1^Σ mainly due to the enhanced $j_{\max}$ of the stack.

In contrast to the out-of-phase mode, no substantial phase shifts $\delta\varphi_k$ that would influence the harmonic content of $V^\Sigma(t)$ were found in the in-phase mode. As a consequence, all higher harmonics add in phase, which results in a doubling of SCJ amplitudes. In comparison to the SUJ, some

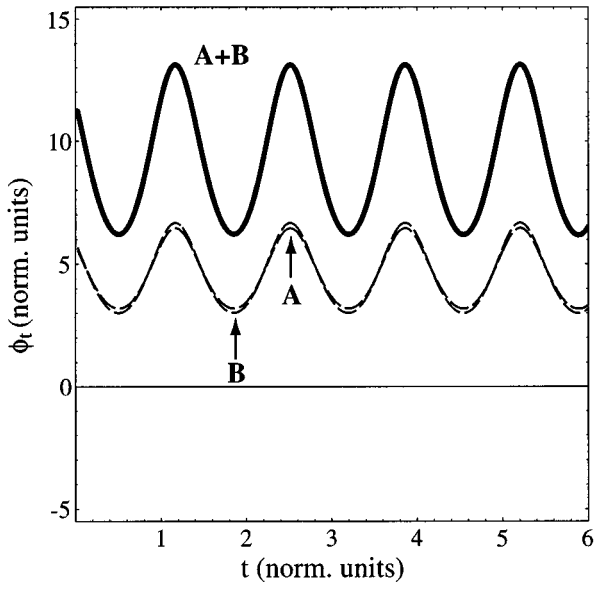

FIG. 21. The temporal evolution of $V^{A,B}(t)$ and $V^{\Sigma}(t)$ in the in-phase flux-flow mode at $\gamma=0.5$ is plotted for $J=j_c^A/j_c^B=2$.

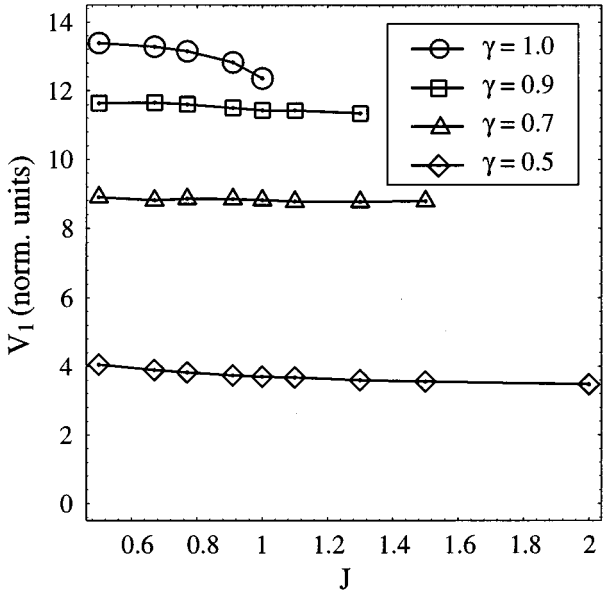

FIG. 23. V_1^{Σ} as a function of the parameter J at constant levels of γ.

gain of the stacked oscillator in in-phase mode can be observed for V_2^{Σ} and V_3^{Σ} as well (see Fig. 19).

The use of LJJ stacks operating in the in-phase flux-flow mode is promising for applications since it increases the amplitudes of all harmonics. The comparison of the total voltage spectrum across the stack with the voltage spectrum of an SUJ shows that, due to the in-phase summation and the magnetic coupling, the first harmonic will be enhanced by a factor of more than 2. Lower harmonics show an increase in amplitude by a factor of between 2 and 1 and the gain is decreasing with the order of the harmonic. The dependence of the gain in the first harmonic amplitude on the spread in critical currents is rather weak, whereas a spread in quasiparticle resistances leads to a decrease in gain.

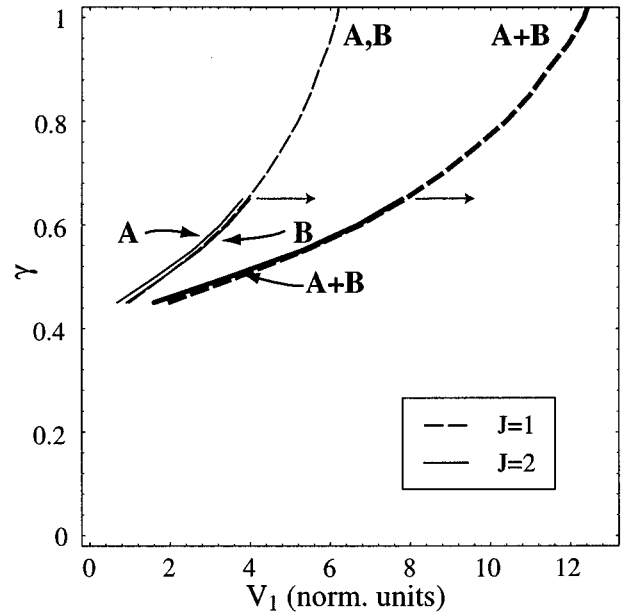

FIG. 22. The first harmonic amplitudes of each single junction ($V_1^{A,B}$) and of the stack (V_1^{Σ}) are plotted as a function of γ for $J=1$ (dashed lines) and $J=2$ (solid lines).

V. CONCLUSION

The ac voltage spectra of double-barrier, stacked LJJs in in-phase and out-of-phase flux-flow modes are studied. In the frame of the theoretical model with frequency independent damping and absence of surface current losses, the out-of-phase flux-flow mode is found to be not feasible for oscillator applications due to low power of all harmonics. Instead, the in-phase flux-flow mode is found to be of high interest for applications that require enhanced power and frequency yield.

The harmonic content of radiation from a twofold coupled stack is governed by the magnetic coupling between junctions, which is inducing magnetic images, and the phase-dependent summation of single junction voltages. We have pointed out the important features of the voltage spectra of the stack in in-phase and out-of-phase modes taking into account differences in the junctions' critical currents and quasiparticle resistances.

The in-phase flux-flow mode provides the possibility to obtain larger power for various harmonics in Josephson radiation. This mode has limited stability and is less robust than the out-of-phase mode with respect to the parameter spread. In experiment it may be stabilized by an accurate tuning to achieve locking.[8] According to our simulations, the in-phase flux-flow mode can be obtained reliably even with rather large spread in critical currents of the junctions. For $\alpha>0.1$, a spread in damping coefficients of about 10% can be tolerated. These limitations can be satisfied by modern Nb/AlO_x technology. Reliability of in-phase locking can be

enhanced by increasing the coupling parameter S, i.e., reducing the thickness of the middle superconducting electrode.

ACKNOWLEDGMENTS

We wish to thank P. Bodin for the permission to use his original numerical code for simulations of coupled LJJs with equal parameters. Helpful discussions with B. A. Malomed are gratefully acknowledged.

[1] V. P. Koshelets, A. V. Shchukin, S. V. Shitov, and L. V. Filippenko, IEEE Trans. Appl. Supercond. **3**, 2524 (1993).
[2] V. P. Koshelets, S. V. Shitov, L. V. Filippenko, A. M. Baryshev, H. Golstein, T. de Graauw, W. Luinge, H. Schaeffer, and H. van de Stadt, Appl. Phys. Lett. **68**, 1273 (1996).
[3] A. Petraglia, A. V. Ustinov, N. F. Pedersen, and S. Sakai, J. Appl. Phys. **77**, 1171 (1995).
[4] A. V. Ustinov, H. Kohlstedt, and C. Heiden, Appl. Phys. Lett. **65**, 1457 (1994).
[5] A. V. Ustinov, and H. Kohlstedt, Phys. Rev. B **54** (1996).
[6] N. Grønbech-Jensen, O. H. Olsen, and M. R. Samuelsen, Phys. Lett. A **179**, 27 (1993).
[7] N. Grønbech-Jensen and J. A. Blackburn, Phys. Rev. Lett. **70**, 1251 (1993).
[8] E. Goldobin, H. Kohlstedt, and A. V. Ustinov, Appl. Phys. Lett. **68**, 1250 (1996).
[9] S. Sakai, P. Bodin, and N. F. Pedersen, J. Appl. Phys. **73**, 2411 (1993).
[10] Robert W. Ramirez, *The FFT, Fundamentals and Concept* (Prentice-Hall, Englewood Cliffs, NJ, 1985).
[11] A. V. Ustinov, T. Doderer, R. P. Huebener, N. F. Pedersen, B. Mayer, and V. A. Oboznov, Phys. Rev. Lett. **69**, 1815 (1992).
[12] Y. S. Kivshar and B. A. Malomed, Phys. Rev. B **37**, 9325 (1988).
[13] E. Goldobin, A. Wallraff, B. A. Malomed, and A. V. Ustinov, Phys. Lett. A (submitted).